Mechanical and Tribological Properties of Electrospun PA 6(3)T Fiber Mats

Matthew M. Mannarino[a] and Gregory C. Rutledge[b,*]

a) Department of Materials Science & Engineering, Massachusetts Institute of Technology, Cambridge, MA 02139

b) Department of Chemical Engineering, Massachusetts Institute of Technology, Cambridge, MA 02139

*Corresponding author. Tel.: +1 617 253 0171; fax: +1 617 258 5766.

E-mail address: rutledge@mit.edu (G. C. Rutledge).

Abstract

The mechanical and tribological properties of electrospun fiber mats are of paramount importance to their utility as components in a large number of applications. Although some mechanical properties of these mats have been reported previously, reports of their tribological properties are essentially nonexistent. In this work, electrospun nanofiber mats of poly(trimethyl hexamethylene terephthalamide) (PA 6(3)T) with average fiber diameter of 463±64 nm are characterized mechanically and tribologically. Post-spin thermal annealing was used to modify the properties of the fiber mats. Morphological changes, in-plane tensile response, friction coefficient and wear rate were characterized as functions of the annealing temperature. The Young's moduli, yield stresses and toughnesses of the nonwoven mats improved by two- to ten-fold when annealed slightly above the glass transition temperature, but at the expense of mat porosity. The coefficient of friction and the wear rate decrease by factors of two and ten, respectively, under the same conditions. The wear rate correlates with the yield properties of the mat, in accord with a modified Ratner-Lancaster model. The variation in mechanical and tribological properties of the mats with increasing annealing temperature is consistent with the formation of fiber-to-fiber junctions and a mechanism of abrasive wear that involves the breakage of fibers between junctions.

Keywords: Electrospinning, Nanofiber, Wear.

1. Introduction

Electrostatic fiber formation, or electrospinning, offers a particularly simple and robust method to create polymeric nanofibers of various morphologies and sizes, inexpensively and in large quantities. In electrospinning, a viscoelastic fluid is charged so that a liquid jet is ejected from the surface of the fluid (typically supplied by a needle or spinneret) and accelerated by an electric field towards a collector, typically a grounded plate, thus creating a nonwoven fiber mat or membrane [1]. Modification of the fiber diameter, porosity, surface area and mechanical properties of the mat by adjusting the processing and solution parameters can be used to tailor electrospun nanofiber mats for various applications. Because of these unique properties and relative ease of fabrication, electrospun fibers and their mats have attracted a significant amount of attention in recent years for a broad range of applications [2,3] including (but not limited to): drug release agents [4], optical sensors [5], and ion-exchange membranes [6,7]. In each of these applications the mechanical response and tribology of the nanofiber mat is likely to be critical to the performance and/or success of the device in service.

Electrospun nanofibers have been reported to exhibit some remarkable increases in elastic stiffness and yield stress for fibers below a critical diameter, whose value varies from material to material [8,9]. The origin of these increases in fiber mechanical properties remains a topic of some debate. Regardless of the diameter-dependent changes in fiber properties, the as-spun mats tend to exhibit consistently low yield stresses (typically 0.5-3 MPa), Young's moduli (typically 20-60 MPa) and toughnesses (typically 0.5-2 MJ/m^3) [10,11]; as-spun untreated nanofiber mats also exhibit low mechanical resilience (<50%) even at small strains of less than 0.02 mm/mm [12]. Occasionally this is an advantage for applications such as tissue engineering where a soft, porous matrix is desirable; however, for many applications of nonwoven mats, modest improvements in the stiffness or mechanical integrity without significant losses in the porosity would be highly desirable to ensure durable and robust performance. Although many experimental studies have been conducted on the mechanical properties of conventional nonwoven fabrics, there are a limited number of reports that account adequately for the observed mechanical properties of mats comprising electrospun nanofibers. In recent years several research groups have demonstrated significant improvements to the Young's modulus and yield stress of electrospun polymeric fiber mats by various forms of post-spinning techniques such as thermal annealing [13], mechanical drawing [14], hot pressing [15], and solvent vapor treatment [16]. Subjecting a semi-crystalline polymer fiber to heat treatment at a temperature above the crystallization temperature (T_c) of that fiber, but below the equilibrium melting temperature (T_m) of the polymer, can cause the melting of small, imperfect crystals, and the formation of larger, more perfect crystals within the fibers, thus creating a stiffer and tougher matrix [17,18]. With some amorphous polymer nonwovens,

annealing has been shown to allow air or gas pockets within the fibers to diffuse out, creating stronger more uniform fibers [19]. In addition, if the heat-treatment of the amorphous polymer nanofiber mats is conducted above the material's glass transition temperature (T_g), deformation and welding between fibers can be observed that would also contribute to changes in mechanical properties due to the increase in the number of junctions, analogous to an increase in the cross-link density of an elastomer.

Various post-spin treatments can improve the mechanical strength and expand the utility of nonwoven nanofiber mats; however, the resistance of electrospun mats to wear remains a significant issue. In order to improve the robustness of nanofiber mats, both mechanical strengthening and tribological tailoring is required to keep the membrane intact. Investigation of the tribological properties of textiles and fabrics is not unprecedented; Derler et al. measured the friction coefficient and hardness of conventional textiles in contact with human skin equivalents [20], and Gerhardt et al. measured the frictional properties and contact pressure of skin-fabric interactions, for example [21]. The textile industry has used various abrasive and wear testing techniques (such as the Taber abraser) to evaluate the durability of fabrics. Such quantitative testing would be invaluable to the development and commercialization of nanofiber mats. Despite the need for improving the wear resistance of nanofiber mats, to our knowledge there has still not been any published investigation of their tribological properties or methods for improvement. Quantitative evaluation of the wear resistance of the nanofiber mats is critical for a better understanding of the trends and underlying mechanism of wear occurring in the nanofiber mats. This work seeks to quantify the tribology of nanofiber mats, and to demonstrate the improvement of mechanical integrity and wear resistance of electrospun mats by post-spinning thermal treatments, to generate robust membranes.

2. Experimental

2.1. Materials

Poly(trimethyl hexamethylene diamine terephthalamide) (PA 6(3)T) was purchased from Scientific Polymer Products, Inc. It is an aromatic, amorphous polyamide with a high glass transition temperature (T_g=425 K) and outstanding mechanical properties. The substituent methyl groups in PA 6(3)T suppress crystallization, yielding an amorphous material at all temperatures that is more soluble in organic solvents and easier to process than semi-crystalline polyamides. As solvent, N,N-dimethyl formamide (DMF) was purchased from Sigma-Aldrich and used as received for creating for creating polymeric solutions. The tensile modulus and yield stress of electrospun PA 6(3)T fibers and mats have been examined in some detail and reported previously [9,22].

2.2. Electrospinning of Nanofiber Mats

Nanofiber mats were fabricated by electrospinning from organic polymer solutions using a parallel plate geometry as shown in Figure **1**. Two aluminum plates, each 12 cm in diameter, were positioned one above the other to achieve a tip-to-collector distance of 25 cm. A high voltage power supply (Gamma High Voltage Research, ES40P) was used to apply an electrical potential of 22 kV to the polymer solution and the top plate. The nozzle consisted of a stainless steel capillary tube (1.6 mm OD, 1.0 mm ID) (Upchurch Scientific) in the center of the top plate. A digitally controlled syringe pump (Harvard Apparatus, PHD 2000) was used to obtain a flow rate of 0.010 mL/min. The jet current was measured as the voltage drop across a 1 MΩ resistor placed in series between the bottom plate and ground (Fluke, 287 true RMS multimeter). The voltage readings were then converted to electrical current using Ohm's law. The entire apparatus was contained within a fume hood to ensure proper ventilation. An anti-stick agent (CP Fluoroglide® from Saint-Gobain Performance Plastics) was sprayed onto the aluminum collector plate to facilitate removal of the electrospun mat.

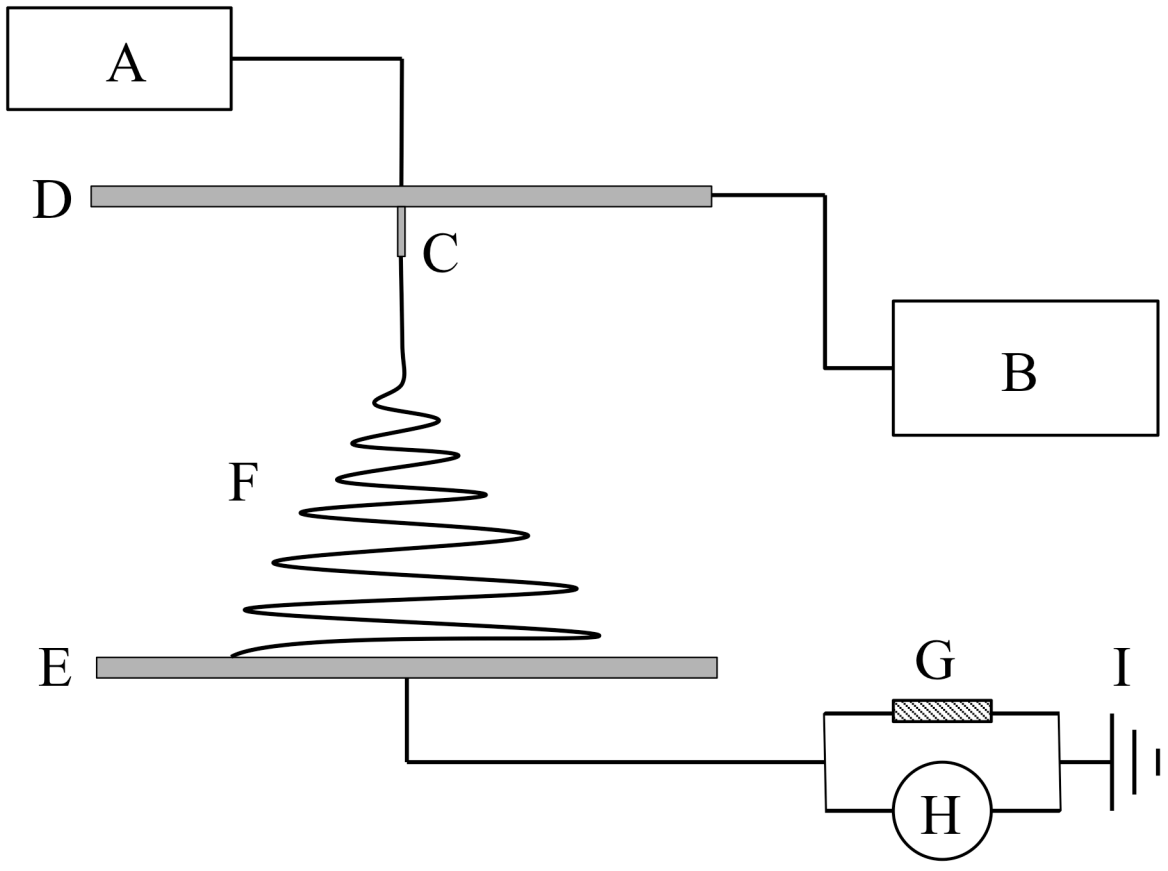

Figure 1. Schematic representation of parallel-plate electrospinning apparatus: (A) solution pump; (B) high voltage power supply; (C) capillary tip; (D) upper plate; (E) lower grounding collector plate; (F) whipping polymer fiber jet; (G) resistor; (H) voltage meter; (I) ground.

2.3. Morphological Characterization of Nanofiber Mats

A JEOL JSM-6060 scanning electron microscope (SEM) was used to determine the diameter and morphology of the fibers. A thin layer of gold (~10 nm) was sputter-coated onto SEM samples prior to imaging. Fiber diameter was determined by taking 100 diameter measurements of the fibers from a set of SEM micrographs at 10,000X magnification using ImageJ, from which the mean value and standard deviation of the mean were calculated. Porosity of the fiber mats was determined gravimetrically by cutting out rectangular sections and measuring the mass and dimensions of the mat specimen and converting to porosity. Sample thickness was measured with a Mitutoyo digital micrometer with a constant measuring force of 0.5 N. Lateral sample dimensions were determined using a digital caliper. The volume and mass of the specimen were then converted to a porosity using the bulk density of PA 6(3)T (1.12 g/cm^3) and the following equations [23,24],

$$\rho_{app} = \frac{m_{mat}}{h_{mat} \times A_{mat}} \quad (1)$$

$$\phi = \left(1 - \frac{\rho_{app}}{\rho_{bulk}}\right) \times 100\% \quad (2)$$

where ρ_{app} is the apparent density, m_{mat} is the mass of mat, h_{mat} is the thickness of mat, A_{mat} is the area of mat, ϕ is the mat porosity (%) and ρ_{bulk} is the bulk density.

2.4. Post-electrospinning Treatment of Electrospun Mats

Heat treatment of the electrospun mats was carried out in a Thermolyne lab oven by draping the mat over a 100 mm diameter pyrex dish and placing it in the oven for 2 hours at a specified temperature. Contact of the mat with the rim of the pyrex dish was sufficient to prevent the mats from contracting and/or tearing during heat treatment and suspended the sample so that it did not contact or stick to any surfaces. After heat treatment, samples were removed from the oven and allowed to cool before carefully cutting the mat off of the pyrex dish.

2.5. Mechanical Testing

Uniaxial tensile testing of electrospun fiber mats was measured with a Zwick Roell Z2.5 tensile testing machine using a 2.5 kN load cell. Rectangular specimens were cut to 100 mm × 12.5 mm and extended at a constant crosshead speed of 0.50 mm/s with a 50 mm gauge length. Five specimens were tested for each temperature of thermal treatment to determine the mean value; error bars on all plots represent one standard deviation of the mean. The thickness of each specimen was determined from the average of three measurements taken along the gauge length with a Mitutoyo digital micrometer with a constant measuring force of 0.5 N. The force–displacement data as taken from the Zwick was converted to engineering stress–engineering strain results. Engineering stress is defined as the ratio of force to the

initial cross-sectional area, and engineering strain is defined as the ratio of the change in length to the original gauge length.

2.6. Tribological Testing

The coefficient of friction was measured according to ASTM D-1894-11 [Standard Test Method for Static and Kinetic Coefficients of Friction of Plastic Film and Sheeting] using a custom-made "sled and spring gauge" apparatus. Friction force measurements were taken at a series of normal forces ranging from 0.25-2.5 N with an IMADA push-pull force gauge (10 N capacity and 0.05 N precision), at a testing speed of 0.25 m/s. Five measurements were taken for each set of heat-treated mats to determine the mean value and standard deviation of the mean. The counter-face used for coefficient of friction measurements was the H-38 Calibrade® standardized abrasion testing wheel used in the abrasive wear testing experiments.

The surface roughness of the nanofiber mats and polymer film were measured using a Veeco surface profiling system, Model "Dektak 150". A 2.5 μm stylus with 3.0 mg tip force was used to scan across 5.0 mm of sample in 30 seconds. The arithmetic average roughness (R_a) was recorded for each sample analysis and the average of five scans was used to determine the mean R_a.

The abrasive wear resistance of the electrospun mats was measured by subjecting the mats to a modified ASTM D-3884-09 [Standard Test Method for Abrasion Resistance of Textile Fabrics (Rotary Platform, Double-Head Method)]. Test samples were prepared by carefully cutting out 100 mm diameter circles from an electrospun mat and attaching them to the adhesive side of a 100 mm diameter Polyken® 339 duct closure foil. This prevents the mats from bunching up or shifting during testing. For comparison, a solution cast film was made by depositing 3.0 mL of 20 wt.% PA 6(3)T in DMF on a 100 mm diameter Kapton® sheet and allowing the solvent to evaporate overnight in a fume hood. Five 100 mm specimens were prepared for each temperature of thermal treatment and for each specified number of abrasion cycles to determine the mean value and standard deviation of the mean. H-38 Calibrade® standardized abrasion testing wheels were used with an applied load of 25 or 100 g for 10, 50, 100, 250, 500, and 1000 cycles at 1 revolution per second (25 cm/s). The H-38 Calibrade® standardized Taber abrasion wheel is classified in ASTM D-3884-09 as a very fine-grained abrasive wheel for use in testing woven and nonwoven fabrics as well as delicate textiles. Samples were analyzed for abrasive wear by visual inspection and mass loss using an Ohaus E11140 analytical balance. By measuring the mass loss of the nanofiber mats after a specified number of cycles (or sliding distance), the effective wear rates of the membranes were determined. With the exception of the as-spun sample, the data for mass loss vs. number of cycles for each sample was fitted to a second order polynomial forced through the origin, using the method of least squares. An effective wear rate for each sample was then calculated by taking

the value of the tangent to the second order polynomial at 100 cycles. The as-spun sample deteriorated too quickly to measure the mass loss reliably beyond the first 50 cycles; therefore, the slope of a linear fit through the first three data points was used in calculating the effective wear rate for the untreated nanofiber mat.

3. Results and Discussion

3.1 Morphology/Porosity of Heat-Treated Mats

Electrospun fibers of PA 6(3)T with diameters ranging from 150 nm up to 3.6 μm and their tensile properties have been reported previously by our group [22]. This order of magnitude variation in fiber diameters was achieved by varying solvent composition and polymer concentration as well as processing parameters. Uniform PA 6(3)T fibers having a mean diameter of 463±64 nm were fabricated from a 22wt% solution of DMF for use in all of the tests described here. Each nonwoven fiber mat was produced using 1.0 mL of polymer solution to generate a mat of roughly 100 μm thickness and 15 cm in diameter. The mats were then heat-treated at various temperatures close to the T_g of PA 6(3)T (~153 °C as determined by differential scanning calorimetry), which we believe serves to increase the number of weld points between fibers as well as remove any residual solvent and air pockets from the interior of the fibers. Figure **2** shows SEM micrographs of PA 6(3)T fibers after 2 hours of heat-treatment at various temperatures spanning a range from below to above T_g. There are no discernable weld points between fibers on the untreated SEM; however at 150 °C thermal treatment, several weld points become visible, with even more weld points at 160 °C. The 170 °C heat-treated nanofiber mat exhibited extensive fusion between fibers, leading to considerable loss of the original fiber morphology and porosity, creating a webbing effect between fibers.

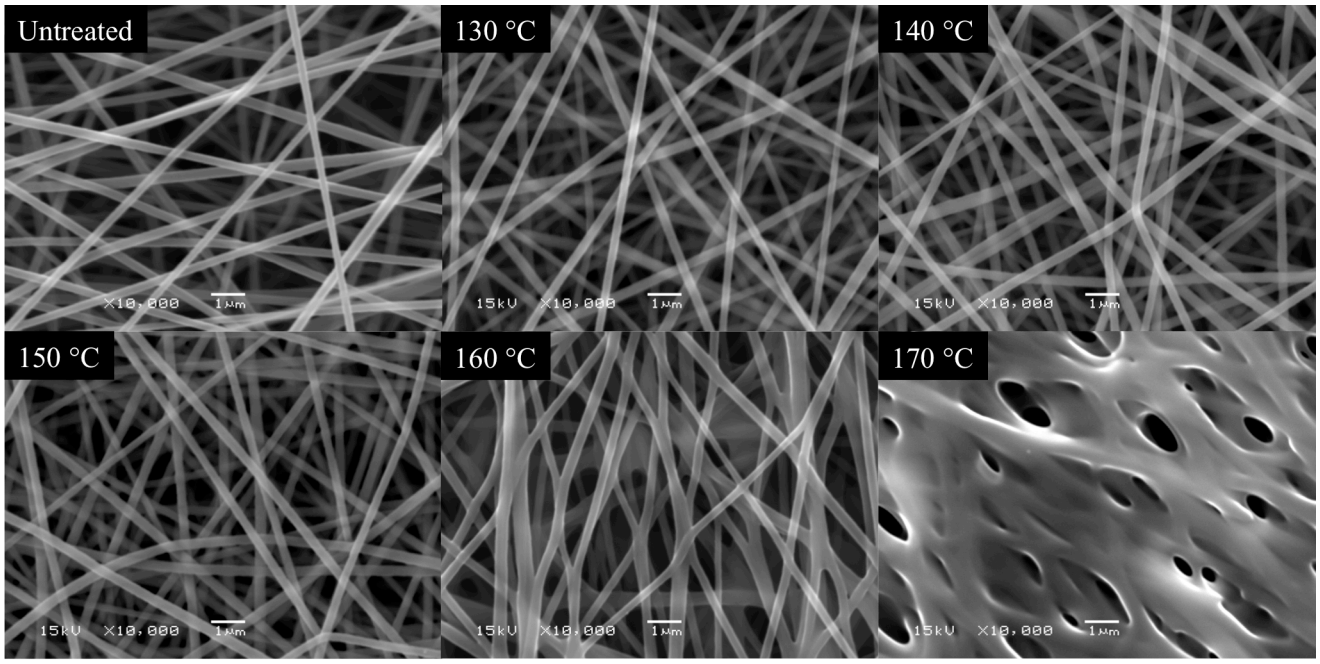

Figure 2. SEM Micrographs of PA 6(3)T nanofibers after varying degrees of heat treatment. From upper left to lower right: untreated, and 2 hours thermal annealing at 130, 140, 150, 160 and 170 °C, respectively. Scale bar for each image is 1 μm.

The SEM micrographs show the decrease in pore size between fibers as the temperature of heat-treatment increases, as well as what appears to be a decrease in the overall porosity of the mats. Before the mats were subjected to the heat-treatment, they were typically 100±10 μm in thickness, and it was observed that for the highest annealing temperature (170 °C), the mats can contract to as thin as 60 μm. Figure **3** shows a plot of the porosity of PA 6(3)T nanofiber mats after various heat treatments. The nonwoven mats have an inherently high as-spun porosity of 88.5±1.1%, which drops slightly to 85.2±1.5% as the result of mild heat treatment (below the T_g of PA 6(3)T). Annealing at temperatures above the T_g produces a significant drop in porosity. The porosity of the sample after annealing at the highest temperature (170 °C) fell to 62.8±5.1%.

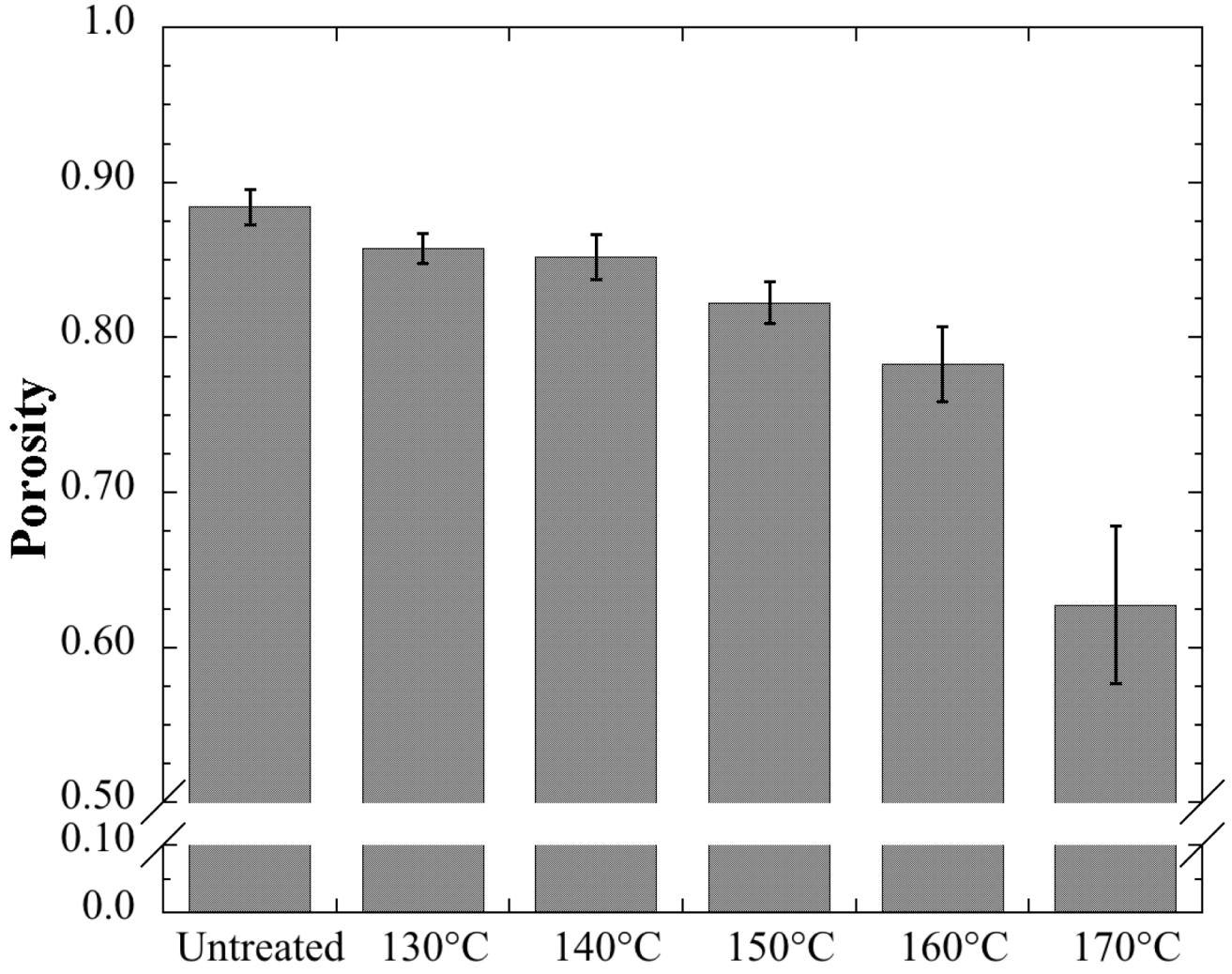

Figure 3. Porosity of PA 6(3)T nanofiber mats after heat-treatment at various temperatures.

3.2. Mechanical Properties of Heat-Treated Mats

Uniaxial, constant strain-rate tensile testing was employed to observe the effect of varying degrees of heat-treatment on the mechanical response of nanofiber mats. Representative plots of the tensile behavior of heat-treated electrospun mats is shown in Figure **4**; note the increase in modulus and yield stress with increasing temperature of heat-treatment and the transition from somewhat ductile-like failure for materials annealed below 150°C, due to the propagation of tears in the fabric, to brittle fracture for those annealed at or above 150 °C.

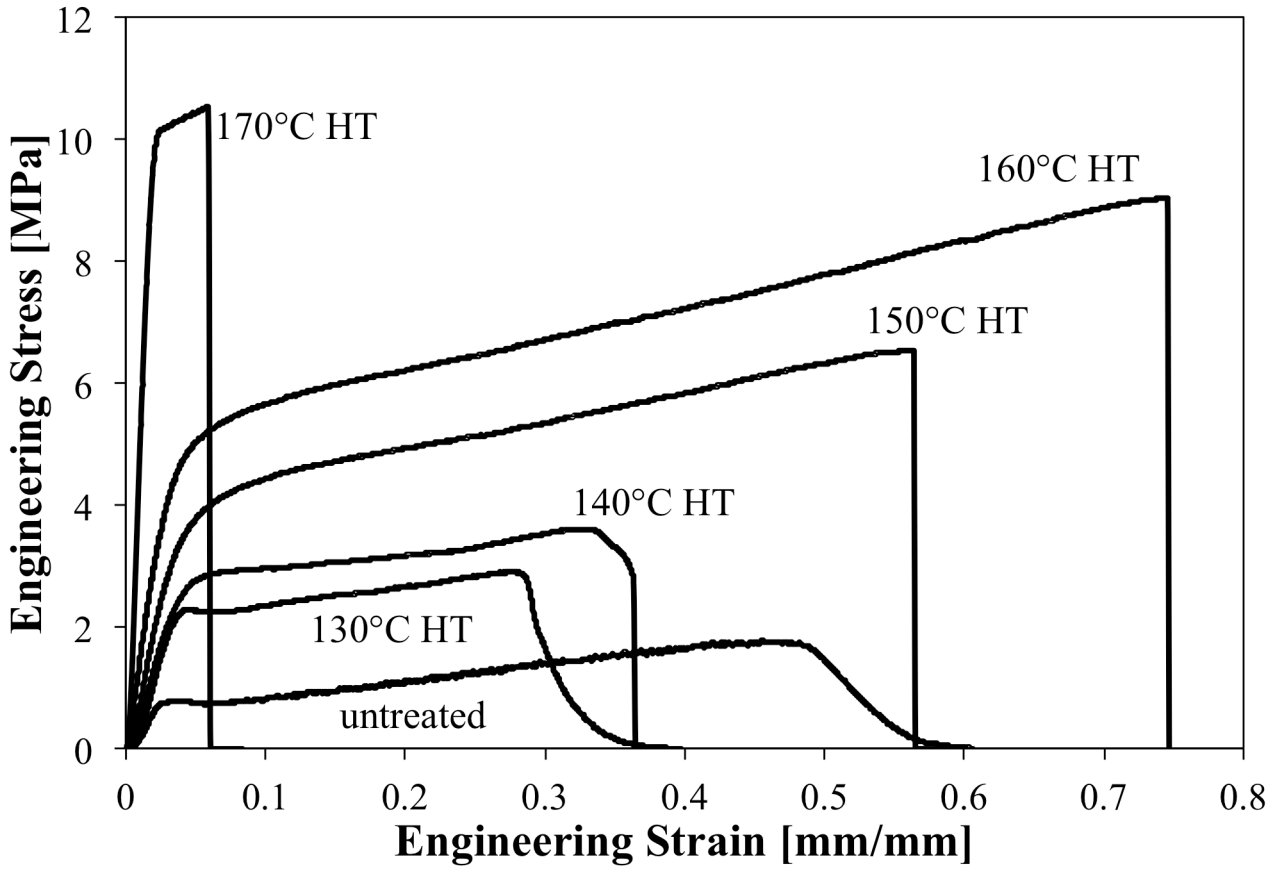

Figure 4. Representative stress-strain curves for PA 6(3)T fiber mats with varying degrees of heat-treatment (2 hours each at 130-170 °C).

Analysis of the results of the nonwoven mat tensile testing show that subjecting the samples to thermal treatment can dramatically improve their mechanical properties. Histograms showing the improvements to the Young's modulus, yield stress, strain at break, and tensile energy-to-break (toughness) are plotted in Figures 5 and 6. The Young's modulus and yield stress for the as-spun material were 40.56 ± 4.82 MPa and 0.75 ± 0.02 MPa, respectively. These results are consistent with those reported by Pai et al for mats comprising fibers with diameters around 400 nm.[9] The Young's modulus and yield stress of the mats increases modestly from the as-spun state to the heat-treated samples below T_g (130-140 °C), then increases even further for samples treated above 150 °C and shoots up dramatically after thermal annealing at 170 °C, as shown in Figure **5**. The histogram for the yield stress looks very similar to the inverse of the trend in porosity shown in Figure **3**, with close to a linear increase in the yield stress for mats up to the 160 °C heat-treated samples, before a sharp jump is observed for the 170 °C treated mat. The plots for strain at break and tensile energy-to-break (shown in Figure **6**) for the nanofiber mats do not follow a simple trend with increasing temperature of heat-treatment. There is a slight drop in the strain at break with the lowest temperature of heat-treatment (130

°C), indicating a possible transition from a ductile fracture response to more brittle behavior; then there is a steady increase in the strain-to-break with increasing heat-treatment, indicating a toughening of the fiber mat that prevents a critical crack from propagating through the sample. The sample annealed at 170 °C breaks very early (<10% strain) and exhibits very little strain after yield, indicating that the material has become very brittle, behaving like a porous film containing large voids that act as stress concentrators to initiate crack formation. The toughness of the heat-treated PA 6(3)T nanofiber mats shows that the as-spun mat and mats annealed at temperatures up to 140°C exhibit low toughness due primarily to their low modulus and yield stress, while the 170 °C HT membrane also has a low toughness due to its small breaking strain. The toughest mats are the ones that have been annealed at a temperature close to the T_g of PA 6(3)T, where there is a significant increase to both the yield stress and the strain-to-break; these mats exhibit a 5-10 fold increase in toughness over the untreated mats.

The changes observed in the mechanical properties of the electrospun mats cannot be explained solely based on changes in mat porosity; for example, a 3.5-fold increase in solidity (=1–porosity) from the untreated sample to that treated at 170°C is accompanied by a change in modulus of over 10-fold. Pai et al [9] previously showed that the distance and curvature of fibers between points of contact ("junctions") with other fibers are also important. The increase in Young's modulus for the heat-treated mats is consistent with thermal welding of the fibers at their junctions, in addition to the reduction in porosity. Using the nonwoven fabric model for curved fibers reported by Pai et al [9] and the values reported there for the fiber modulus and radius of curvature of PA 6(3)T fabrics comprising 407 nm fibers (*c.f.* Table 2 of Ref 9), we calculate distances between junctions that decrease from about 17.5 μm for the as-spun mats to 14.1 μm for the mats heat-treated at 160°C. This corresponds to an increase in junction density, and is at least qualitatively consistent with the images shown in Figure **2**.

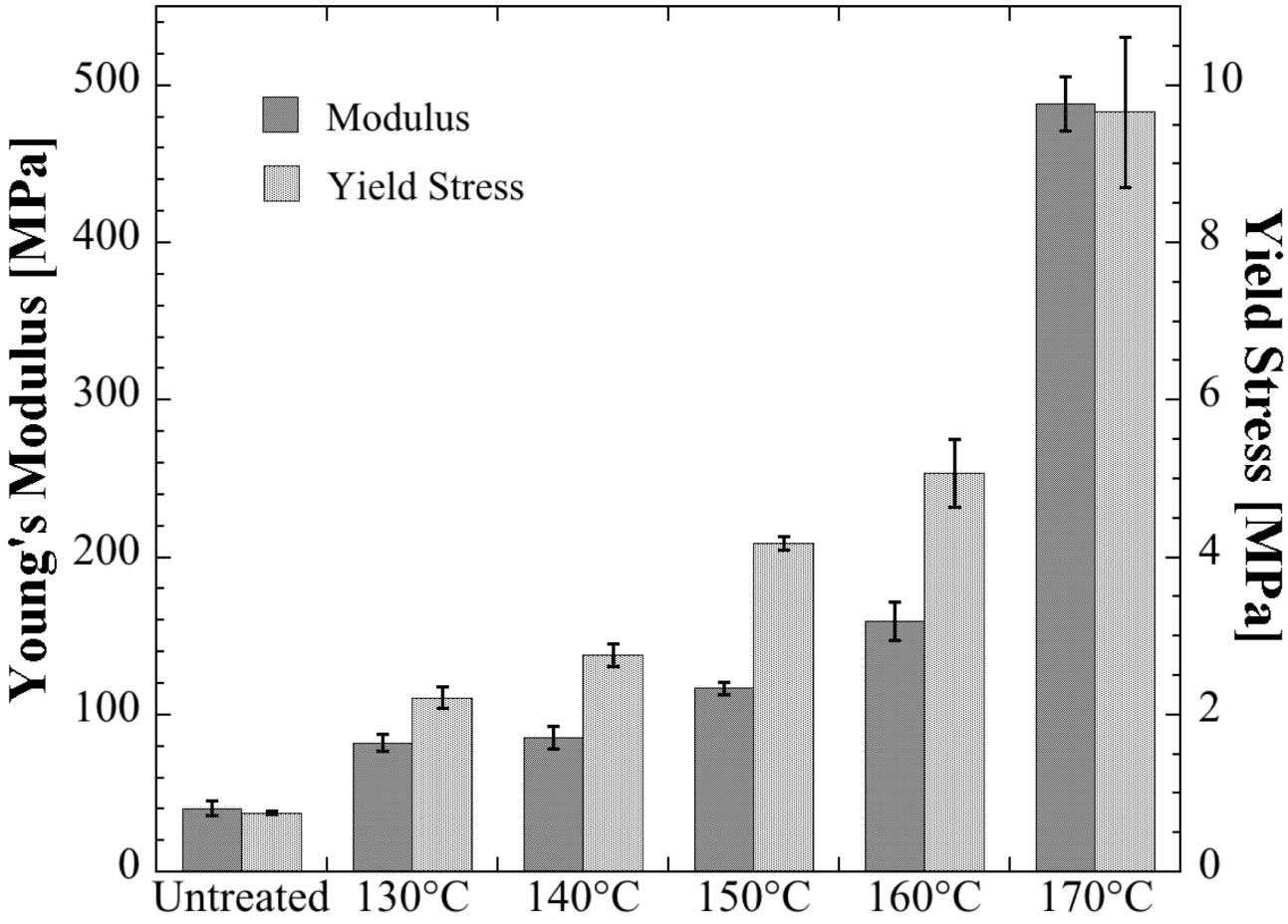

Figure 5. Plot of Young's modulus and yield stress vs. temperature of heat-treatment for PA 6(3)T nanofiber mats.

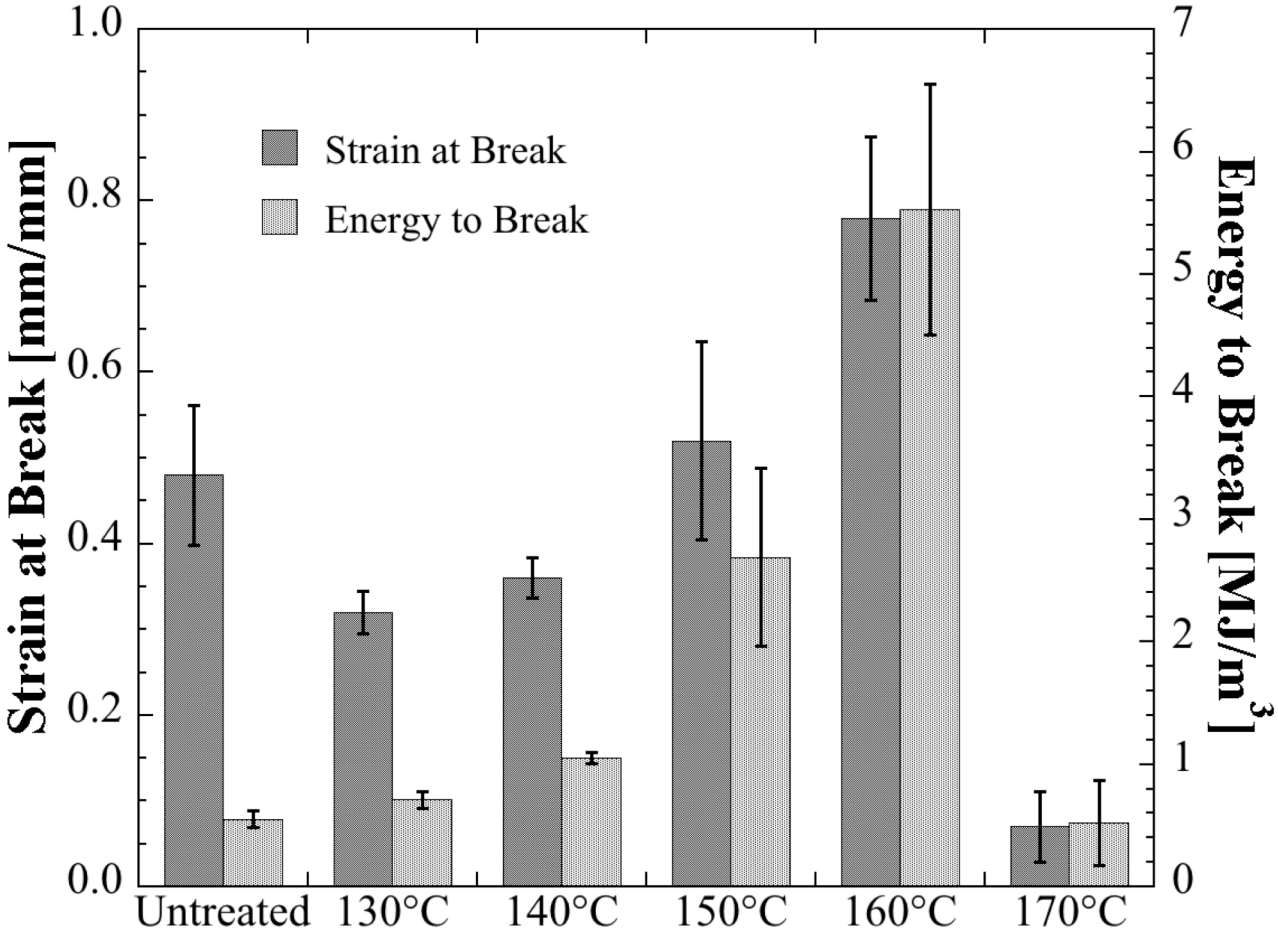

Figure 6. Plot of the strain-to-break and tensile energy-to-break vs. temperature of heat-treatment for PA 6(3)T nanofiber mats.

The mechanical resilience of a mat is often of paramount importance for many applications such as filtration, fiber scaffolding, or sensors where the membrane would be subjected to repeated small strain deformations that could result in catastrophic failure if the membrane were not resilient enough to recover. Single load-unload strain cycle tensile testing was performed to determine the resilience of the nanofiber mats and what effect thermal treatment has on the mechanical hysteresis. Representative mechanical hysteresis tensile loops for up to 4% engineering strain are shown in Figure **7**. The area between the extension curve and recovery curve is a measure of the total energy dissipated over the 4% strain cycle, which when normalized by the toughness yields a measure of the hysteresis of the material. The hysteresis of the heat-treated PA 6(3)T nanofiber mats at single cycle strains of 0.02, 0.04, and 0.10 mm/mm are plotted in Figure **8**. A sharp decrease in hysteretic losses of the nanofiber mats is observed with samples annealed close to the T_g, especially at low strains. This indicates that thermal annealing can improve elastic recovery from low strain deformation. Nanofiber mats treated above the T_g began to exhibit an increase in the mechanical hysteresis, indicating that there is some trade-off between the

morphological changes that occur during thermal treatment and the resilience of the nanofiber mats. The hysteresis behavior at large strain (10%) is not as drastically affected by the thermal annealing as the low-strain behavior, but modest improvements are still observed with heat-treated fiber mats at 140-150 °C (near the T_g of PA 6(3)T).

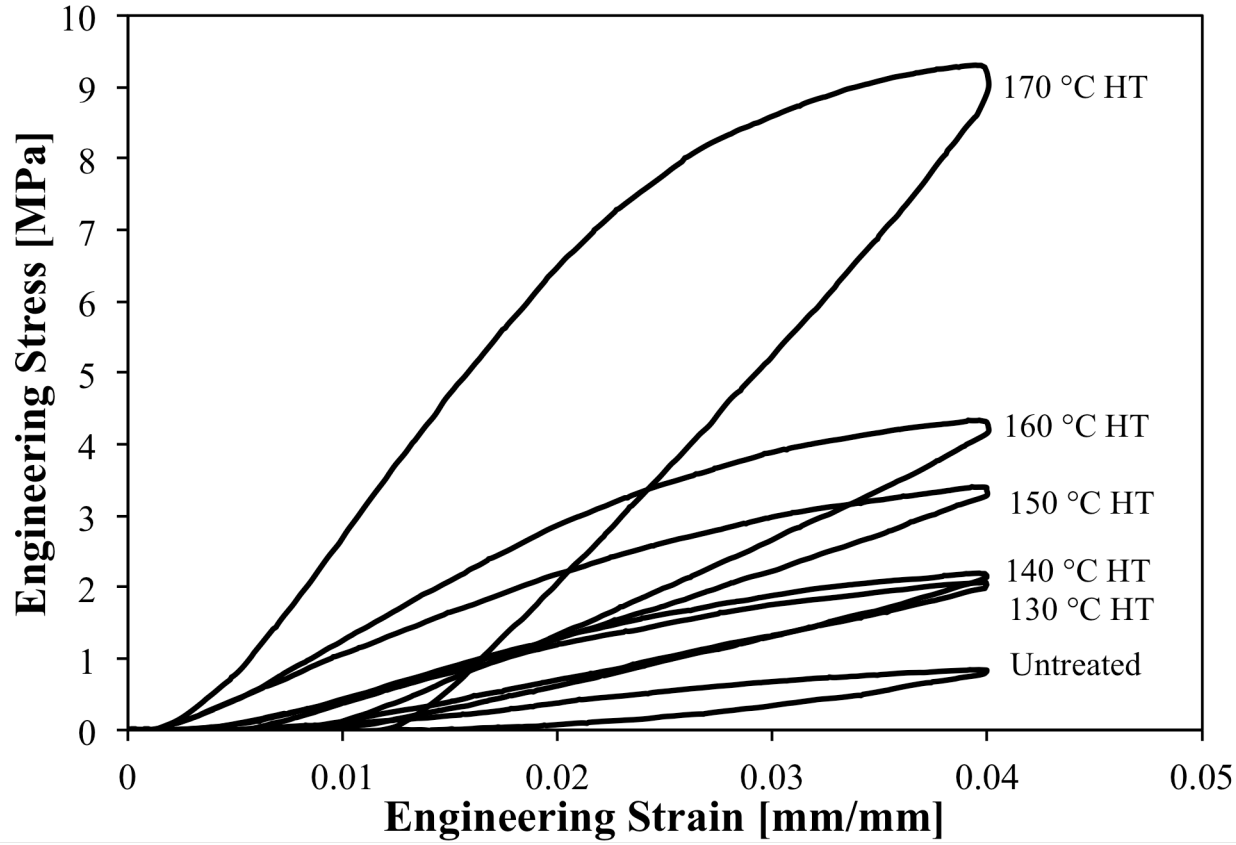

Figure 7. Representative 4% strain mechanical hysteresis tensile loops for PA 6(3)T fiber mats with varying temperatures of heat-treatment (2 hours each at 130-170 °C).

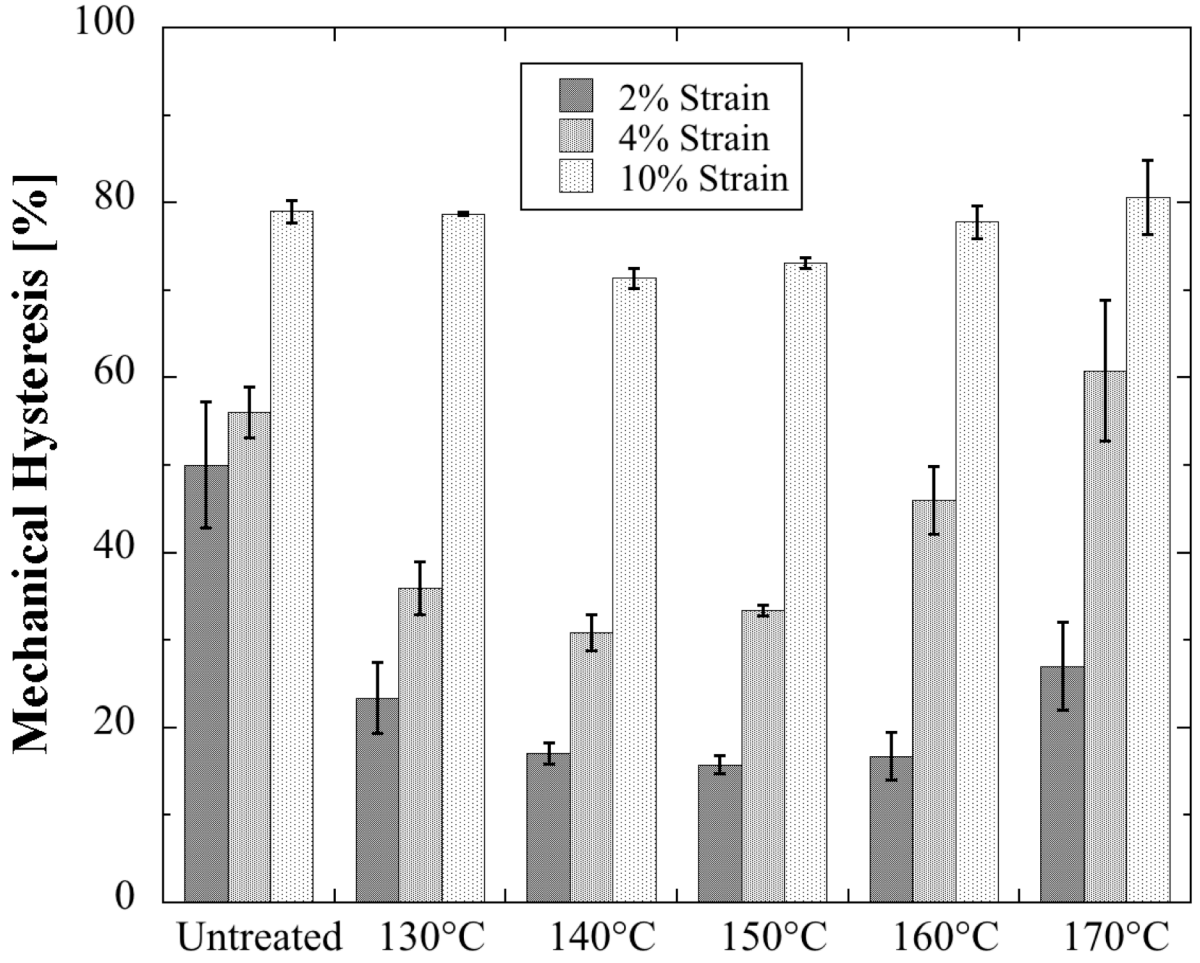

Figure 8. Plot of mechanical hysteresis at 2, 4, and 10% strain vs. temperature of heat-treatment for PA 6(3)T nanofiber mats.

3.3. Tribology of Electrospun Mats

Electrospun fiber mats are typically fragile and susceptible to wear and delamination even under conditions of gentle handling. This is a concern for the post-spin processing as well as the end-use of such mats and could be a critical limitation to their service lifetime. To quantify this behavior, the coefficient of friction was measured using a standardized testing material (Calibrade® H-38 abrasive wheel) for each of the nanofiber mats, as-spun and after each of the prescribed temperatures of heat treatment. For comparison, the coefficient of friction (μ) was measured for the film of PA 6(3)T cast from solution as well. A plot of the friction force vs. the normal force for each temperature of thermal treatment is shown in Figure **9**; from this plot, the friction coefficient can be determined by taking the ratio of the average measured friction force to the applied normal force. A plot of the coefficient of friction vs. the normal force is shown in Figure 10; note that there is a modest decrease in the coefficient of friction with increasing normal force at low loads, but that above 1 N (~100 g applied load), the

coefficient of friction is approximately constant, especially for the samples annealed at or above 150 °C, as would be expected for typical extruded or cast polymer film samples. The decrease in coefficient of friction with increasing load is typical of compressible polymeric materials, whose shear strength increases with applied load [25]. Mean friction coefficients at 100 g load decreased from 0.86 for the as-spun mat to 0.77 for the 130 °C heat-treatment sample, to 0.49 for the 150 °C heat-treated mat, quickly approaching the coefficient of friction for the cast film (0.45). A lower mean coefficient of friction for the nanofiber mats is typically desirable as it implies that the mat experiences smaller forces during abrasive contact with a counter-face, which could lead to significantly less wear.

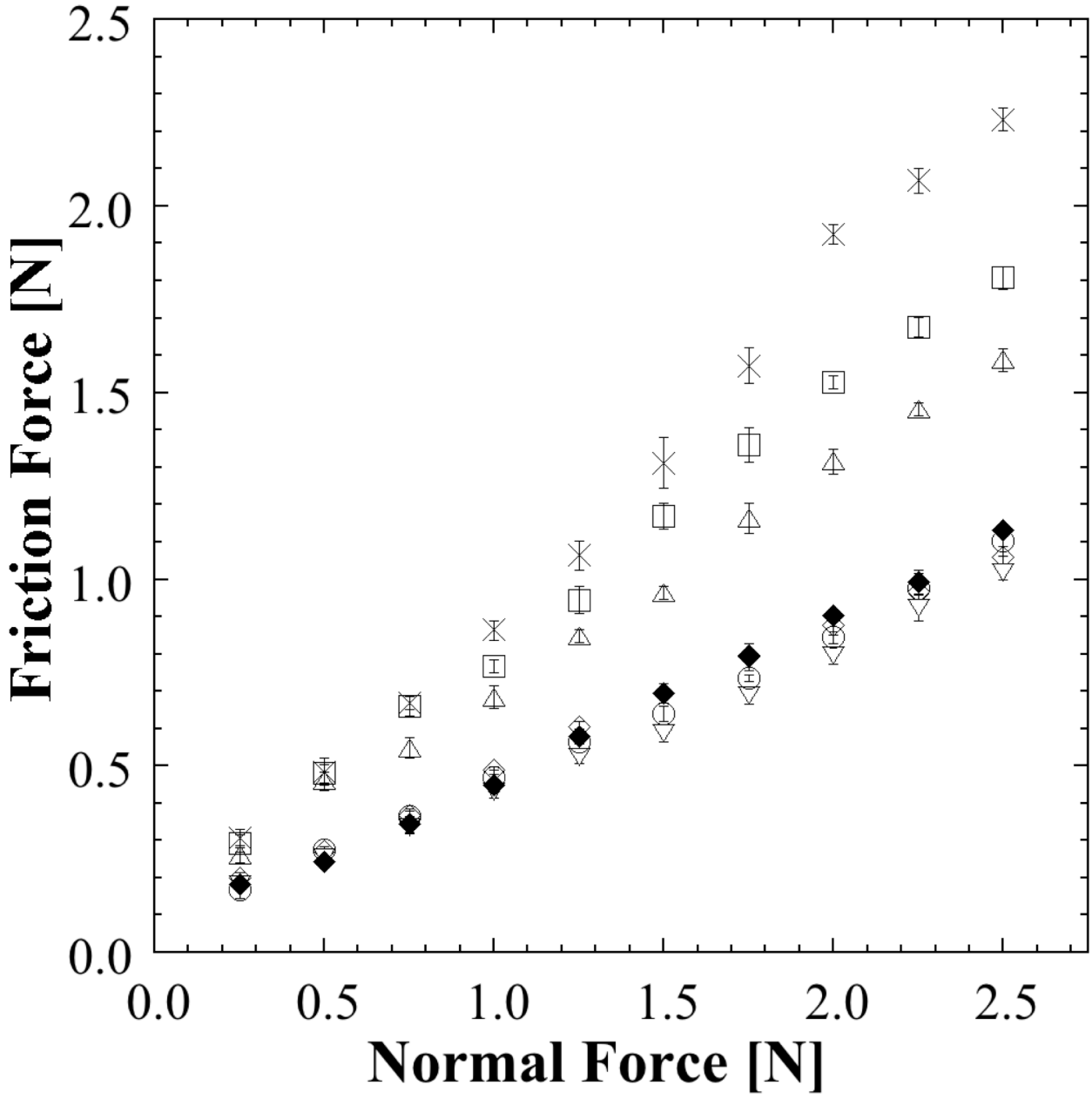

Figure 9. Friction force of PA 6(3)T mats as a function of the normal force with varying temperature of heat-treatment: untreated (×), 130 °C (□), 140 °C (△), 150 °C (◇), 160 °C (▽), 170 °C (○), and cast film (◆).

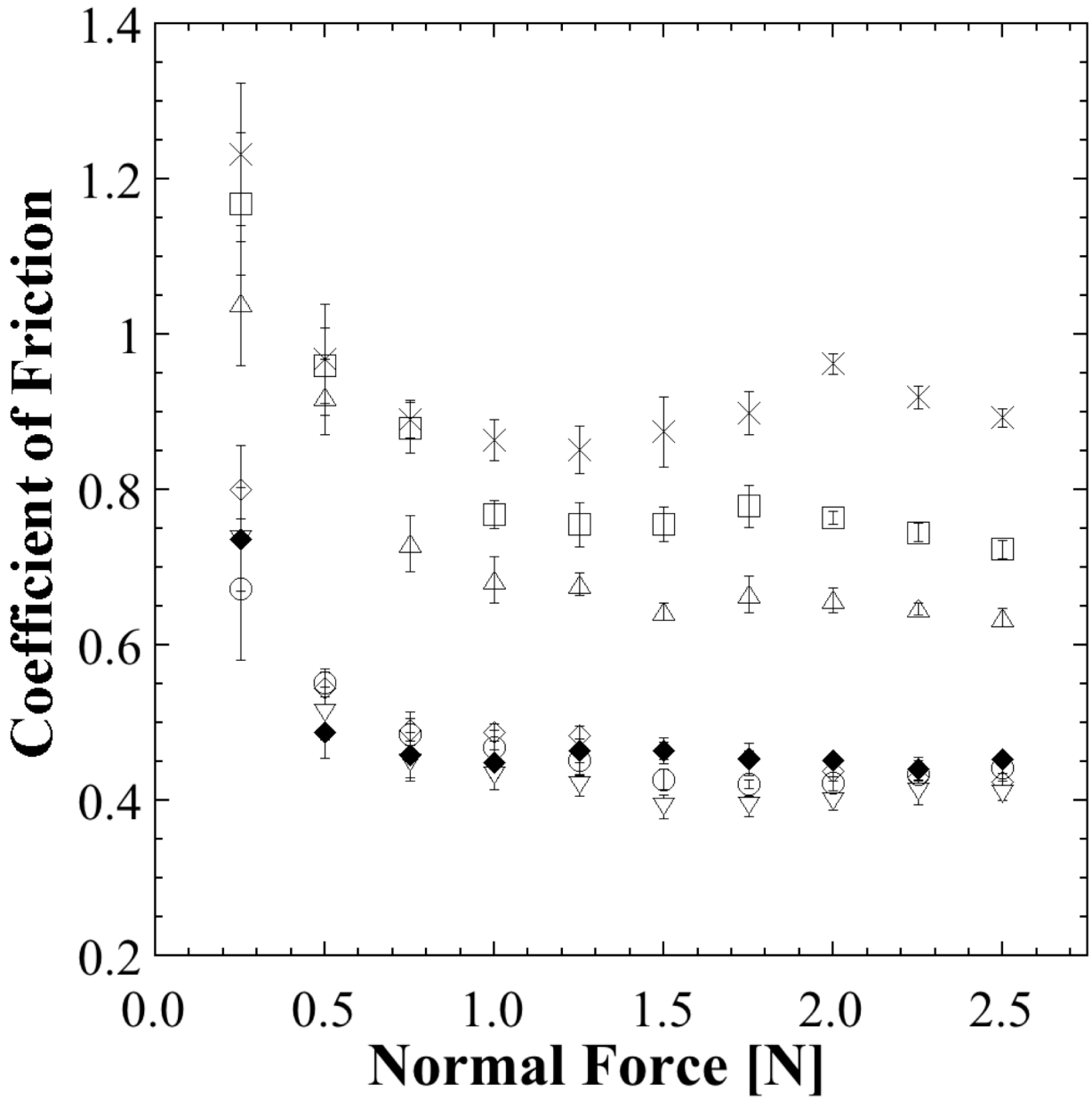

Figure 10. Coefficient of Friction of PA 6(3)T mats as a function of the normal force with varying temperature of heat-treatment: untreated (×), 130 °C (□), 140 °C (△), 150 °C (◇), 160 °C (▽), 170 °C (○), and cast film (◆).

The Taber abraser was used to provide uniform, low levels of abrasive wear in order to accurately measure quantitative changes in the tribological response of thermally treated nanofiber mats. All of the mats had a mean-value roughness (R_a) on the order of 1.0-2.3 μm, and the cast film had a R_a of ~0.15 μm. 100 g applied load was used for the first set of testing because it was the lowest load where the mean friction coefficient for each sample had stabilized to an approximately constant value. Visual inspection of the nonwoven membranes after 10, 50, and 100 abrasion cycles qualitatively indicated

significant differences in the wear mechanisms between the samples annealed at the various temperatures, as shown in Figure **11**. The untreated PA 6(3)T sample exhibits an observable amount of wear and distortion after as few as 10 abrasion cycles, and significant levels of deformation and wear after 50 cycles; the sample is completely destroyed (>50% of sample mass removed from the wear path) before reaching 100 cycles. The 150 °C heat-treated sample is significantly more robust, and exhibits only minor wear and abrasive tears at 10-50 cycles, before enduring more significant tearing and delamination after 100 cycles. The 170 °C heat-treated PA 6(3)T samples were even more robust, showing almost no signs of wear at all until 50 abrasion cycles, then exhibiting some moderate levels of tearing after 100 cycles. The cast PA 6(3)T film exhibited almost negligible wear under the same conditions even up to 100 abrasion cycles.

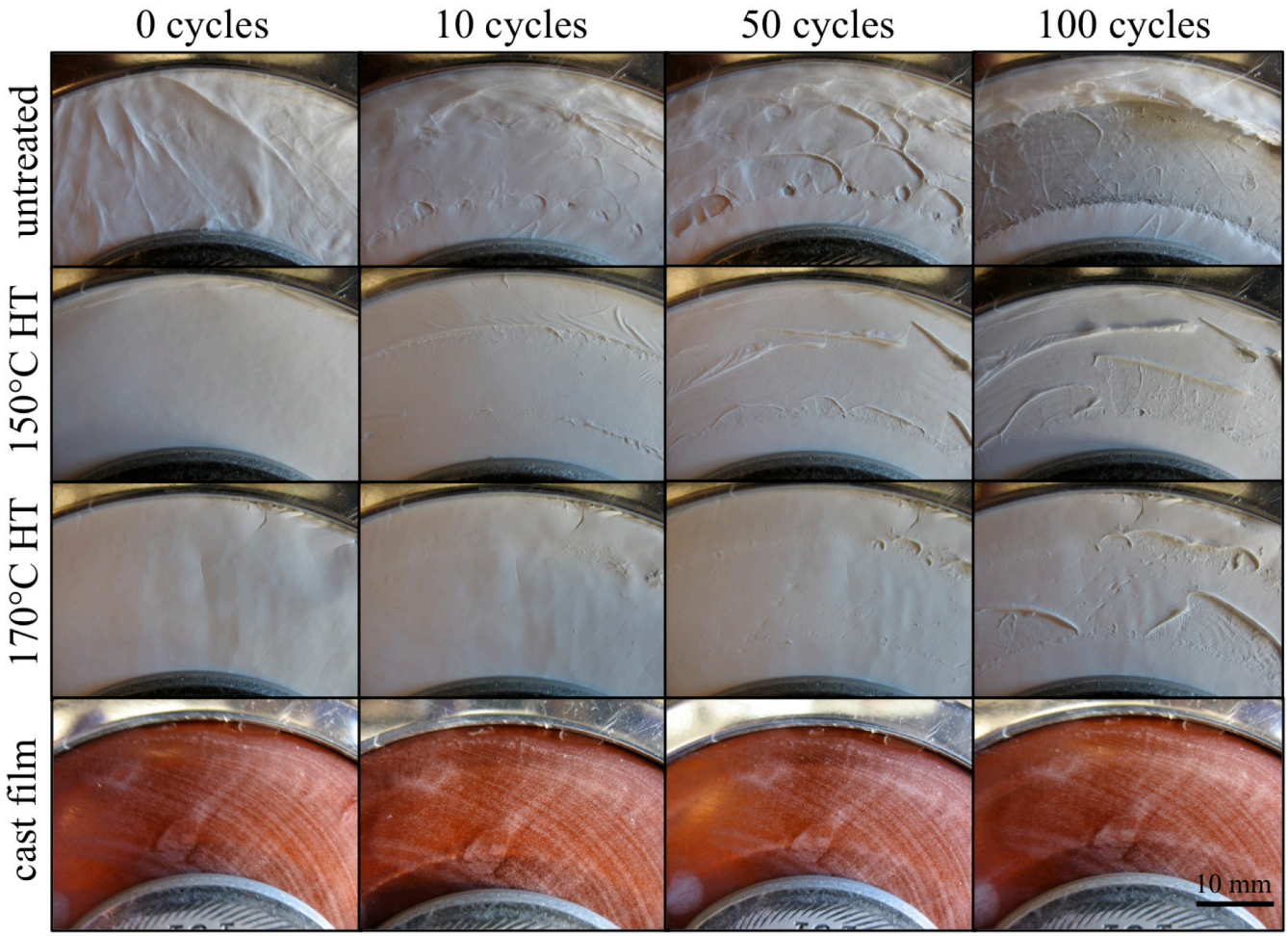

Figure 11. Optical images of abrasive wear path for nanofiber mats at 0, 10, 50, and 100 wear cycles under 100 g applied load (top row: as-spun; second row: 150 °C heat-treated; third row: 170 °C heat-treated, bottom row: cast film), scale bar is 10 mm. Note that the PA 6(3)T cast film is transparent and attached to a brown Kapton® polyimide film for support. The white marks seen in these images are indicative of a light haze that forms within the film during solvent evaporation. These are not surface defects, as confirmed by profilometry.

The change in the coefficient of friction as a function of the number of abrasion cycles would indicate how much the surface of the material is changing over time when subjected to abrasive wear. A plot of the friction coefficient vs. number of cycles with a 100 g load is plotted in Figure **12** for 10, 50, 100, 250, 500, and 1000 cycles. The coefficient of friction for the untreated mat and the 130 °C heat-treated mat both increase significantly after a minimal number of wear cycles, indicating that the surface of the mat is changing with each wear cycle. The mats heat-treated at 140 and 150 °C exhibit a less sharp increase in the coefficient of friction as a function of the number of abrasion cycles; the coefficients of friction appear to level off after approximately 100 cycles. The mats annealed at 160 and 170 °C do not exhibit significant changes to the friction coefficient as a function of the number cycles, even out to 1000 cycles; a similar effect is observed for the coefficient of friction of the PA 6(3)T cast film.

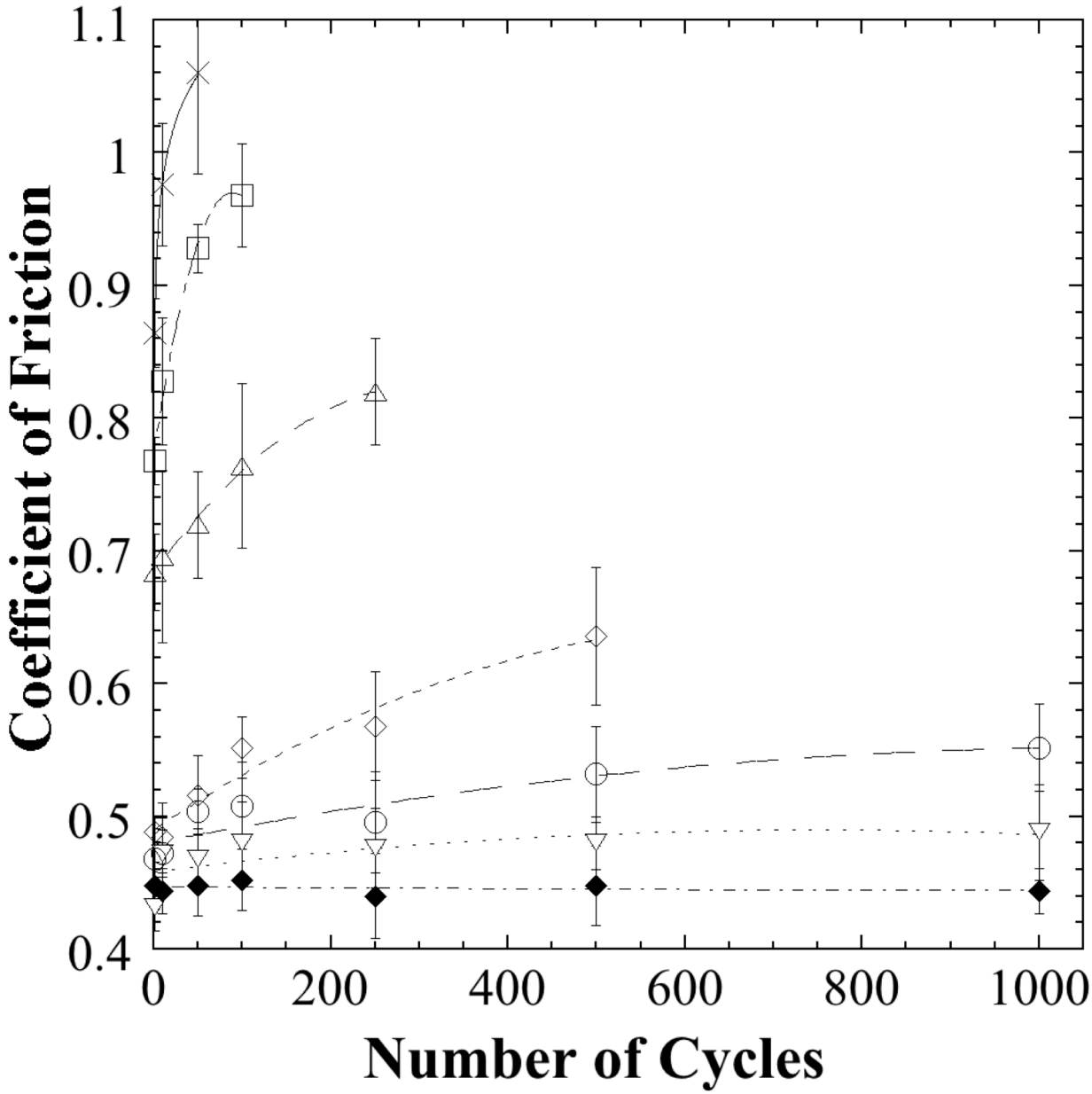

Figure 12. Coefficient of Friction of PA 6(3)T mats as a function of the number of abrasion cycles at 100 g applied load with varying temperatures of heat-treatment: untreated (×), 130 °C (□), 140 °C (△), 150 °C (◇), 160 °C (▽), 170 °C (○), and cast film (◆).

A plot of the abrasive mass loss vs. the number of cycles for 100 g applied load is shown in Figure 13 for 10, 50, 100, 250, 500, and 1000 cycles. The wear rate was measured up to approximately 50% mass loss within the wear path, or ~35-40 mg for each sample. The wear profiles for the nanofiber mats correlate well with the wear behavior of conventional polymer films.

The wear results for the samples under 100 g applied load were adequate for the mats that were annealed above 140 °C; however, since the untreated and 130 °C heat-treated nanofiber mats were

completely destroyed by 100 abrasion cycles, a lighter applied load of 25 g was used to evaluate the less wear-resistant nonwoven mats. The plot of the abrasive mass loss vs. number of cycles for the 25 g applied load is shown in Figure 14. Similar trends for the progression of wear for each sample are seen for the 25 g load as was seen with 100 g applied load, though the effective wear rate for each sample is less. A summary of all the tribological data is compiled in Table 1. Note that for both the 25 g and 100 g applied load, there is nearly an order of magnitude improvement to the effective wear rate of the 150 °C heat-treated nanofiber mat as compared to the as-spun untreated PA 6(3)T mat; however this wear rate is still about an order of magnitude higher than the effective wear rate of the PA 6(3)T cast film.

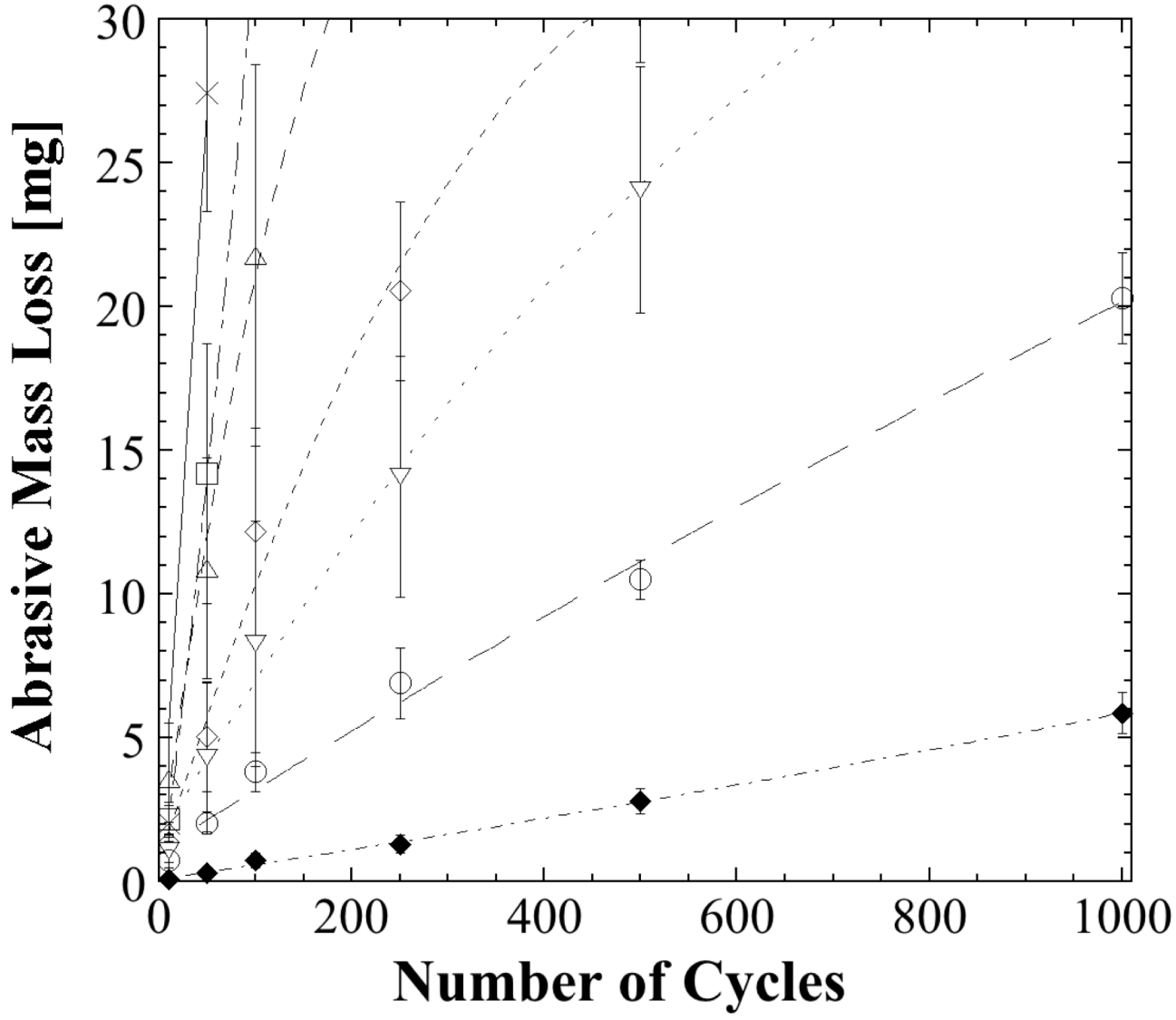

Figure 13. Abrasive mass losses of electrospun nanofiber mats as a function of the number of wear cycles under 100 g load: untreated (×), 130 °C (□), 140 °C (△), 150 °C (◇), 160 °C (▽), 170 °C (○), and cast film (◆).

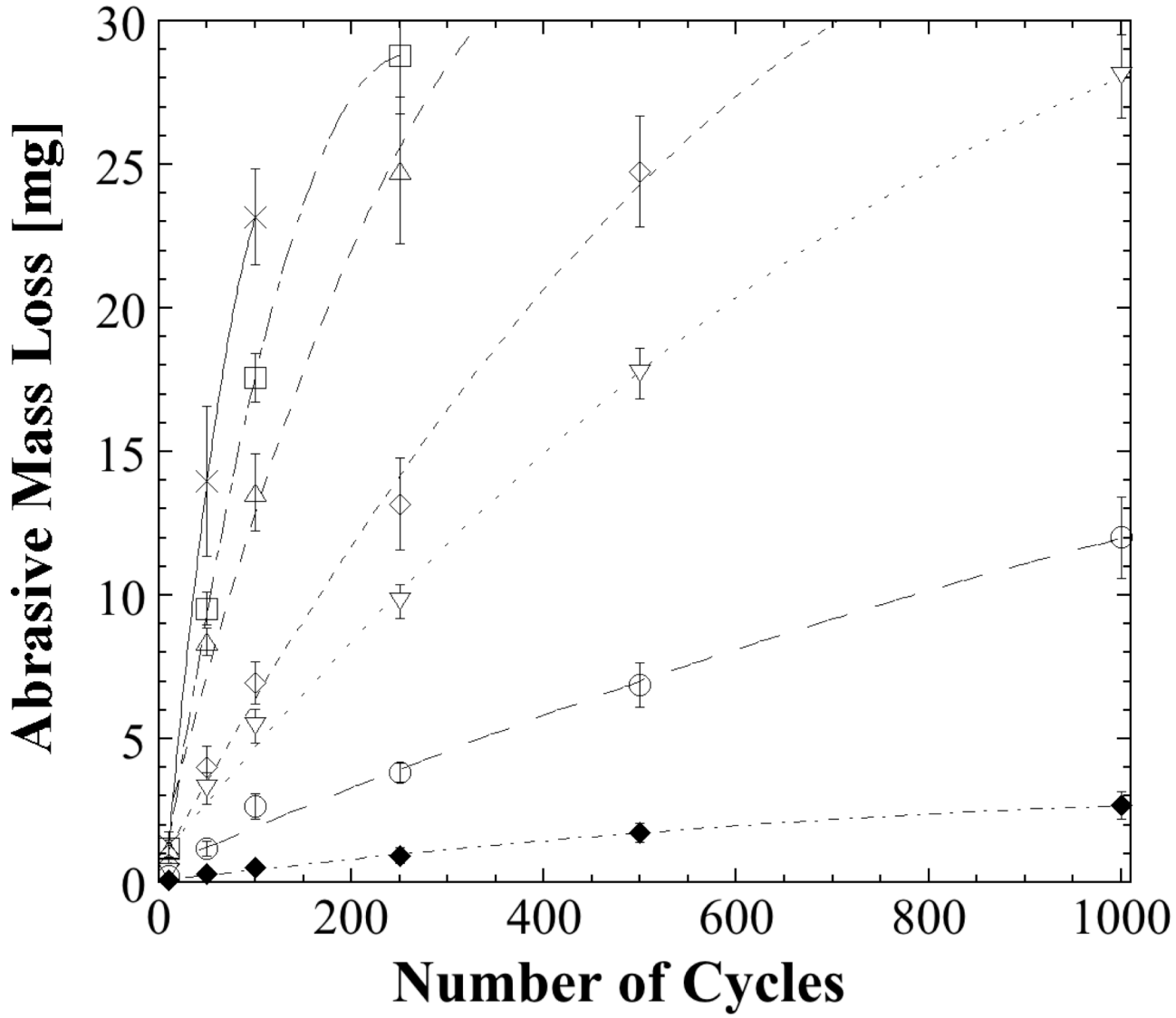

Figure 14. Abrasive mass losses of electrospun nanofiber mats as a function of the number of wear cycles under 25 g load: untreated (×), 130 °C (□), 140 °C (△), 150 °C (◇), 160 °C (▽), 170 °C (○), and cast film (◆).

Table 1. Summary of Tribological Properties of PA 6(3)T Nanofiber Mats

	R_a [μm]	Coefficient of friction, μ (25 g)	Wear Rate (25g) [g/cm]	Coefficient of friction, μ (100 g)	Wear Rate (100g) [g/cm]
Untreated	1.162	1.23	6.38×10^{-6}	0.86	2.14×10^{-5}
130 °C HT	1.030	1.17	5.30×10^{-6}	0.77	1.74×10^{-5}
140 °C HT	2.321	1.04	4.06×10^{-6}	0.68	6.64×10^{-6}
150 °C HT	2.304	0.80	2.32×10^{-6}	0.49	3.66×10^{-6}
160 °C HT	1.478	0.74	1.62×10^{-6}	0.43	2.37×10^{-6}
170 °C HT	1.036	0.67	6.40×10^{-7}	0.47	1.01×10^{-6}
PA 6(3)T film	0.156	0.74	1.62×10^{-7}	0.45	2.19×10^{-7}

The increased effective wear rate observed for the untreated nanofiber mat and samples treated below 150 °C could have a strong correlation with the previously observed increase in the friction coefficient of the mats with number of abrasion cycles (from the plot in Figure **12**). There appear to be large morphological changes in the surface of the nanofiber mats (especially the untreated, 130 °C, and 140 °C heat treated samples) with increasing number of wear cycles as indicated by the sharp increase in the friction coefficient after 10, 50, and 100 cycles. As more mass is removed per cycle with these samples, there could be a significant amount of fiber distortion and debris accumulation that would consequently roughen the surface and increase the coefficient of friction. It was observed when conducting the wear tests that some fibrous debris would transfer from the sample to the abrading wheel during testing (this was removed between each sample run), and some of the fibers and debris would most likely be re-deposited into the pore spaces within the nanofiber mat. Observable residual fibrous debris on the abrading wheel was most prominent for the untreated nanofiber mats as well as the 130 °C and 140 °C thermally treated samples, which were also the samples with the largest increases in friction coefficient.

Determining the mechanism of friction and wear of polymeric nanofiber mats could prove to be vital to the ability to tailor the tribological properties of nonwovens. The mechanism of wear can be due to physicochemical interactions, asperity interactions, or macroscopic deformation [25]. All of the nanofiber mat samples used in this work consist of identical chemical composition, similar fibrous morphology, and comparable surface roughness; therefore, the mechanism of abrasive wear for these nanofiber mats is most likely due to macroscopic deformation caused by exceeding the yield stress of the mats. Relationships between the mechanical properties and wear properties of materials have been investigated before, and some strong correlations have been drawn for polymeric materials based on microscopic and macroscopic wear models [26] In the abrasive wear of polymers, deformation of a

surface is generally a function of the indentation hardness, the relative motion opposed by the frictional force, and disruption of material at the contact points involving an amount of work equal to the area under the stress-strain curve. These three processes occur sequentially, and therefore, the total wear should be proportional to a product of the hardness, the frictional force, and the work (energy) of material removal. One of the most commonly used correlations based on this mechanism is the Ratner-Lancaster correlation [27], which predicts the wear rate, W as:

$$W = C\left(\mu \frac{L}{H\sigma_b\varepsilon_b}\right) \tag{3}$$

where C is a constant, μ is the coefficient of friction, L is the applied load, H is the hardness, σ_b is the breaking stress of the material, and ε_b is the breaking strain. This relationship includes a term for the indentation hardness of a material; however, for most polymers the dominant parameters have been determined to be σ_b & ε_b [28,29]. For nanofiber mats, we suggest that the breaking stress and breaking strain of individual fibers is reflected in the yield stress and strain of the nonwoven mats; therefore, we propose a modified version of the Ratner-Lancaster relationship in which the yield stress, σ_y, and yield strain, ε_y, of the mat replace the breaking stress and strain of the fibers. The wear rate is furthermore put on a mass basis by the bulk density of PA 6(3)T, ρ, to get:

$$W \propto \left(\frac{\rho\mu L}{\sigma_y\varepsilon_y}\right) \tag{4}$$

Figure 15 compares the effective wear rates of the treated nanofiber mats to the modified Ratner-Lancaster wear rate relationship from equation 4 and confirms that there is a strong correlation between the wear rate and the quantity $(\sigma_y\varepsilon_y)^{-1}$ for both the 25 g and 100 g applied loads. The effective wear rate for the PA 6(3)T nanofiber mats is seen to increase logarithmically with $(\rho\mu L)/(\sigma_y\varepsilon_y)$ for over an order of magnitude in these quantities. These results show that the mechanical and tribological properties of nanofiber mats are inter-related and are well-described by conventional abrasive wear correlations modified to reflect the yield behavior of fibrous mats.

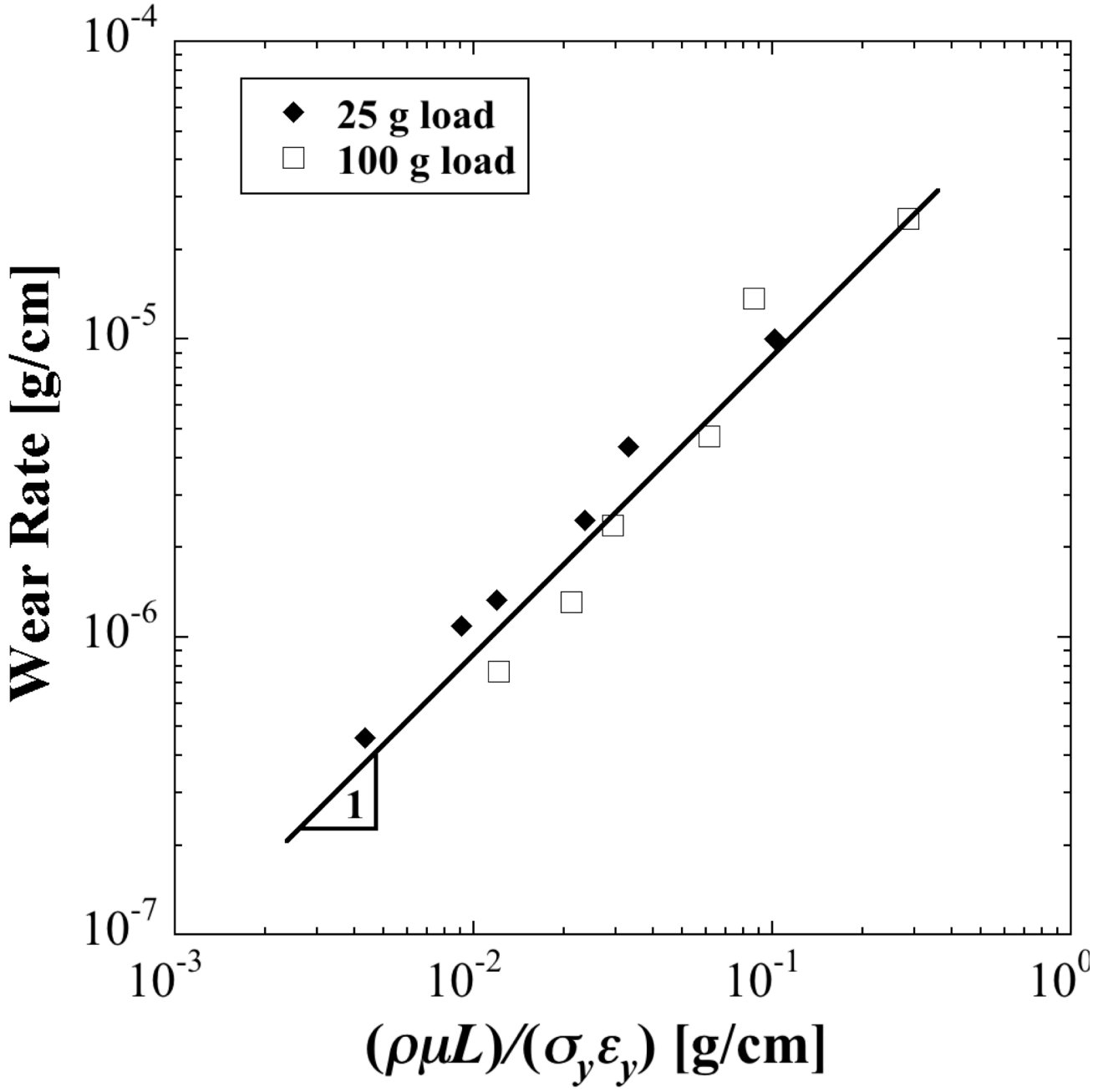

Figure 15. Effective wear rate vs. $(\rho\mu L)/(\sigma_y\varepsilon_y)$ of nanofiber mats subjected to varying temperatures of thermal treatment: (◆) 25 g applied load for wear, (□) 100 g applied load wear. The line with slope=1 is drawn as a guide to the eye.

4. Conclusions

The tribological and mechanical response of thermally treated electrospun nanofiber mats were investigated in this work. The Young's moduli and yield stresses of the nonwoven mats were found to improve dramatically with an increase in the temperature of heat-treatment at or above the glass

transition temperature, at the expense of mat porosity. The Young's modulus increased significantly from 40 MPa for the untreated PA 6(3)T nanofiber mat, to 82 MPa and 117 MPa after 130 °C and 150 °C heat-treatment, respectively, without suffering a significant loss of porosity; the modulus could be increased further to >400 MPa after 170 °C heat-treatment, but at a substantial loss to the mat porosity (88% to 63%). The annealed nanofiber mats also exhibited less mechanical hysteresis under low-strain deformations than the as-spun mat, indicating that the heat-treated mats can recover more readily and have significantly improved fatigue resistance. In addition to gains in mechanical integrity, there was also an improvement in the wear resistance of the nanofiber mats with thermal treatment. Annealing at 150°C results in an order of magnitude decrease in the effective wear rate relative to that of the as-spun mats, from 2.14 x 10^{-5} g/cm to 2.19 x 10^{-6} g/cm at 100 g applied load, while the porosity decreases only modestly, from 88% to 82%. The effective wear rate of nanofiber mats was well-described by a modified Ratner-Lancaster relationship for wear rate of polymeric materials, $W \sim (\rho \mu L)/(\sigma_y \varepsilon_y)$, suggesting that the mechanism of wear is primarily due to the breakage of fibers that is also responsible for yield in these nonwoven mats. Post-spin treatments such as thermal annealing close to the relevant thermal transition temperature (e.g. the glass transition) serve to weld the fibers to form additional fiber junctions, significantly improving the mechanical and tribological properties of the electrospun mats and greatly improving their utility and service lifetime.

Acknowledgements

Funding for this work was provided by the National Science Foundation through grant number CMMI-0700414, the Masdar Institute, and the U.S. Army through the Institute for Soldier Nanotechnologies (ISN) under AROW911NF-07-D-0004. The authors would like to thank Prof. Stephen Burke Driscoll and the Plastics Engineering Department at the University of Massachusetts Lowell for use of their Taber abraser and discussions about wear testing of textiles. The authors would also like to acknowledge the Hammond lab at MIT for use of their Dektak surface profiling system, and the MIT Institute of Soldier Nanotechnology for use of facilities.

References

[1] Doshi J, Reneker DH, Journal of Electrostatics 1995;35(2):151-160.
[2] Flemming RG, Murphy CJ, Abrams GA, Goodman SL, Nealey PF, Biomaterials 1999;20(6):573-588.
[3] Matthews JA, Wnek GE, Simpson DG, Bowlin GL, Biomacromolecules 2002;3(2):232-238.
[4] Kenawy ER, Bowlin GL, Mansfield K, Layman J, Simpson DG, Sanders EH, Wnek GE, Journal of Controlled Release 2002;81:57-64.
[5] Wang XY, Drew C, Lee SH, Senecal KJ, Kumar J, Samuelson LA, Journal of Macromolecular Science-Pure and Applied Chemistry 2002;A39(10):1251-58.
[6] Choi J, Lee KM, Wycisk R, Pintauro PN, Mather PT, Journal of Power Sources 2008;180(1): 167-171.
[7] Bajon R, Balaji S, Guo SM, Journal of Fuel Cell Science Technology 2009;6(3):031004.
[8] Li L, Bellan LM, Craighead HG, Frey MW, Polymer 2006;47(17):6208-6217.
[9] Pai CL, Boyce MC, Rutledge GC, Polymer 2011;52(26):6126-6133.
[10] Jin HJ, Chen HS, Karageorgiou V, Altman GH, Kaplan DL, Biomaterials 2004;25(6):1039-1047.
[11] Zong XH, Ran SF, Fang DF, Hsiao BS, Chu B, Polymer 2003;44(17):4959-4967.
[12] Silberstein MN, Pai CL, Rutledge GC, Boyce MC, Journal of the Mechanics and Physics of Solids 2012;60(2):295-318.
[13] Wang X, Zhang K, Zhu M, Hsiao BS, Chu B, Macromolecular Rapid Communications 2008;29(10):826-831.
[14] Lai C, Zhong G, Yue Z, Chen G, Zhang L, Vakili A, Wang Y, Zhu L, Liu J, Fong H, Polymer 2011;52(2):519-528.
[15] Na H, Zhao Y, Zhao C, Zhao C, Yuan X, Polymer Engineering And Science 2008;48(5):934-940.
[16] Jeong L, Lee KY, Liu JW, Park WH, International Journal of Biological Macromolecules 2006;38(2):140-144.
[17] Gao K, Hu X, Dai C, Yi T, Materials Science & Engineering B 2006;131(1):100-105.
[18] Cho D, Zhmayev E, Joo YL, Polymer 2011;52:4600-4609.
[19] Pai CL, Boyce MC, Rutledge GC, Macromolecules 2009;42(6):2102-2114.
[20] Derler S, Schrade GU, Gerhardt LC, Wear 2007;263:1112-1116.
[21] Gerhardt LC, Mattle N, Schrade GU, Spencer ND, Derler S, Skin Research and Technology 2007;14(1):77-88.
[22] Pai CL, Boyce MC, Rutledge GC, Polymer 2011;52(10):2295-2301.
[23] He W, Ma ZW, Yong T, Teo WE, Ramakrishna S, Biomaterials 2005;26(36):7606-7615.
[24] Zhu X, Cui W, Li X, Jin Y, Biomacromolecules 2008;9(7):1795-1801.
[25] Suh NP, Tribophysics, 1st ed. New Jersey: Prentice-Hall, 1986.
[26] Budinski KG, Wear 1997;203:302-309.
[27] Lancaster JK, Wear 196914(4):223-239.
[28] Wang A, Sun DC, Stark C, Dumbleton JH, Wear 1995;181:241-249.
[29] Shipway PH, Ngao NK, Wear 2003;255:742-750.